

## Narrow Band Numerical Path Loss Models for Wireless Leadless Cardiac Pacemaker Application

Xiao Fang, Xufeng Du, Qiong Wang, and Dirk Plettemeier

Chair of RF and Photonics Engineering, Communication laboratory, TU Dresden, Dresden, Germany

### Abstract

In this paper, we investigate the intra-cardiac to subcutaneous and intra-cardiac to off-body path loss models in three potential sub-GHz narrow bands, i.e., MICS Band (402 – 405 MHz), WMTS Band (608 – 614 MHz) and ISM Band (867 – 869 MHz), for the wireless leadless cardiac pacemaker (LCP) applications. In view of computational efficiency and accuracy, a simplified 4-Cole-Cole model is studied and utilized for the tissues in and surrounding the cardiac region. Then, based on the anatomical human numerical model, the path loss values of intra-cardiac to subcutaneous and intra-cardiac to off-body are calculated, and the corresponding path loss models are fitted with log-distance model. The derived path loss models are useful factors in the analysis and design of the wireless LCP communication system and medical Internet of Thing networking.

### 1 Introduction

The development of body area communication and implantable medical devices brings lots of advancements for the patients, such as less invasive than traditional wired solutions, more effective diagnosis and etc. Cardiac pacemaker, as one of the most important and popular implantable devices, can help control abnormal cardiac rhythms. The conventional pacemaker consists of a subcutaneous device connecting with the electrodes implant inside the right atrium and right ventricle by leads. The leadless pacemakers are expected to replace all the leads by the wireless connections. As shown in Fig. 1, two LCPs are directly implanted in the right atrium and right ventricle respectively and wirelessly synchronize with each other. They will directly communicate with the off-body device or relayed via the subcutaneous implanted node.

Path loss models are useful planning tools that allow wireless communication network design and power consumption management. There are several research works in the path loss modeling involving different frequency bands. In [2], the propagation of a plane wave in UWB (3.1 -10.6 GHz) from off-body to the heart is investigated, in which it shows the power attenuation versus with the frequency and the depth of implant. The signal transmission characteristics in blood and cardiac tissue have been assessed between 100 kHz and 1 MHz in [3]. Taking into the consideration of the antenna, the in-vitro and in-vivo experiments are implemented in [4] for

investigating the in-body and off-body channel modeling for the leadless pacemakers at 2.4 GHz.

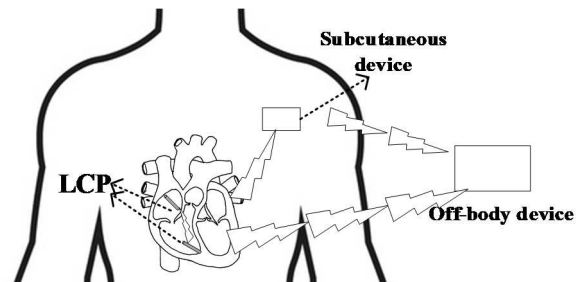


**Figure 1.** Communication modes and position schematic of leadless pacemakers.

The human body as a heterogeneous medium consisting of different tissues with frequency-dependent permittivity and conductivities. Especially, the blood and cardiac muscle as the high-water content tissues will cause large loss for the RF signals. For the in-body to subcutaneous communication, the signal must propagate through different tissues, which will result in reflection and scattering between adjacent tissue layers. Our research focuses on the derivation of the path loss models for the intra-cardiac to subcutaneous communication and intra-cardiac to off-body communication of leadless pacemakers at the potential narrow bands including MICS Band (402 – 405 MHz), WMTS Band (608 – 614 MHz) and ISM Band (867 – 869 MHz).

### 2 Dielectric Properties of Human Tissues

In order to investigate the wave propagation inside human body, building the accurate frequency-dependent models to evaluate the dielectric properties of human tissues are necessary. Based on the measurement and theory models proposed by Gabriel [4]. The 4-Cole-Cole model is one of the most prevalence-accepted models used to approximate the electrical characteristics of human tissues:

$$\epsilon_r(\omega) = \epsilon_\infty + \sum_{n=1}^4 \frac{\Delta\epsilon_n}{1 + (j\omega\tau_n)^{1-\alpha_n}} + \frac{\sigma_0}{j\omega\epsilon_0} \quad (1)$$

where  $\epsilon_\infty$  is the relative permittivity  $f \rightarrow \infty$ ,  $\tau$  is the relaxation time and  $\alpha_n$  is used to describe deviation from Debye behavior. For electromagnetic simulation, 4-Cole-Cole requires too much computational cost so that one-relaxation or two-relaxation modified Debye

approximation are always utilized to fit the human body property in higher part of potential frequency band. The below is one-relaxation modified Debye model:

$$\hat{\epsilon}_r(\omega) = \epsilon_\infty + \frac{\Delta\epsilon_1}{1 + j\omega\tau_1} + \frac{\sigma_0}{j\omega\epsilon_0}. \quad (2)$$

The approximation model is one term of 4-Cole-Cole model excluding  $\alpha_n$ . Based on 4-Cole-Cole and modified Debye model, we investigate the dielectric properties of human tissues in sub-one GHz frequency bands (0.1 GHz-1GHz) which cover all the potential frequency bands. Fig. 2 shows the comparison of dielectric properties, calculating based on three-order relaxations model and four-order relaxations model, of heart. It is obvious that with the frequency increasing, the relativity permittivity decreases and conductivity increases. To reduce the calculation complex, as illustrated in Fig. 2, the three-order relaxations model can be appropriate in the sub-one GHz frequency bands.

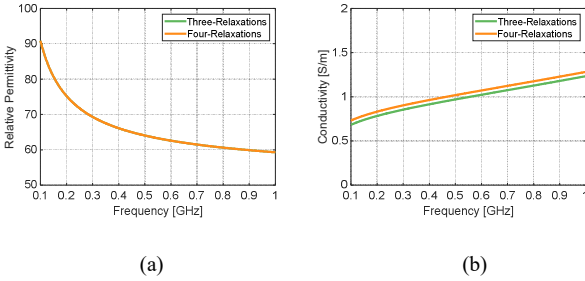


**Figure 2.** (a) Relative permittivity of heart tissue varying with frequency; (b) Conductivity of heart tissue varying with frequency.

For the intra-cardiac to subcutaneous and off-body channels, the electrometric fields propagate through several tissue layers, including blood, heart, muscle, fat and dry skin. The comparison of dielectric properties of these tissues is illustrated in Fig. 3. The high-water content tissue, such as muscle, heart and blood, are with high relativity permittivity and conductivity compared with the low-water content tissue, such as dry skin and fat.

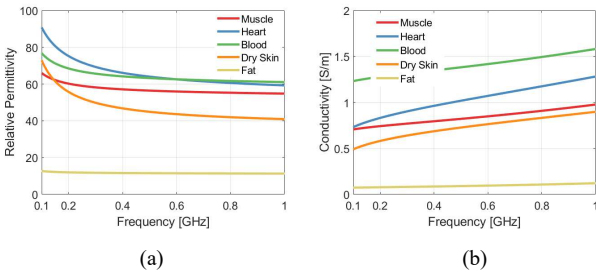


**Figure 3.** (a) Relative permittivity of different tissues varying with frequency; (b) Conductivity of different tissues varying with frequency.

### 3 Numerical Simulation

The numerical simulation is conducted with the CST Microwave Studio. An anatomical human model, named Gustav provided by CST Voxel Family, is utilized as the working environment of leadless pacemaker in the simulation, as shown in Fig. 4. Limited by the size of the pacemaker capsule, the employed antenna is electric small antenna which has far-field radiation similar with Hertzian dipole. Thus, the transmitting antenna is represented by Hertzian dipole, for simplicity, to exclude the mismatch and structure of real antenna. Three different orientations of Hertzian dipole, along x, y and z-axis, are simulated to get a polarization averaged path loss model. The ideal electric and magnetic probes are applied for detecting the electric and magnetic fields at different locations.

Based on the leadless pacemaker application scenario, the transmitting antenna is positioned at the vertex of right ventricle where the pacemaker capsule is also located in reality, as shown in Fig. 4 (a). For the intra-cardiac to subcutaneous model, as shown in Fig. 4 (b), the probes are placed 2 cm below the skin surface under the left collar bone of the human body and is regarded as the actual placement site for the subcutaneous device. Fig 4 (c) illustrates the intra-cardiac to off-body scenario, the probes are positioned a few centimeters away from the body surface in front of the chest, where the receiver station would be located.

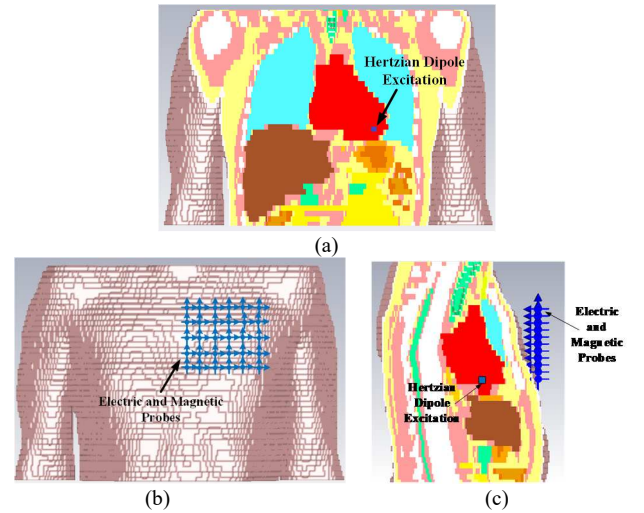


**Figure 4.** (a) The location of transmitting antenna (Hertzian dipole source); (b) The location of receiving antennas (electric and magnetic probes) for the intra-heart to subcutaneous path loss models; (c) The location of receiving antennas (electric and magnetic probes) for the intra-heart to off-body path loss models;

The power intensity at each position is calculated by the pointing vector as following:

$$S_{(x,y,z)}(t) = E_{(x,y,z)}(t) \times H_{(x,y,z)}^*(t). \quad (3)$$

where  $E_{(x,y,z)}(t)$  and  $H_{(x,y,z)}(t)$  are the time-domain electric and magnetic field vector intensities. The average received power at a single position is determined from all three x, y, z polarized electric and magnetic probes. Finally, the path loss is calculated from the ratio of averaged receiving power at the observation point to the transmitted power. The numerically calculated data can be fitted to the following log-distance model with log normal shadowing:

$$PL_{dB} = PL_{0,dB} + 10n \lg\left[\frac{d}{d_0}\right] + N(0, \sigma_{dB}). \quad (4)$$

where  $PL_{0,dB}$  is the path loss at the distance  $d_0$  and  $n$  is the path loss exponent. The cumulative distribution function (CDF), which is approximated by a lognormally distributed random variation  $N(0, \sigma)$  with zero mean and standard derivation  $\sigma$ .

The path loss values and fitted model of the intra-cardiac to subcutaneous channel are shown in Fig. 5 and Fig. 6, the parameters are summarized in Table 1. The range of distance from transmitting antenna to the receiving antenna is approximate from 6 cm to 13 cm, which is similar with the practical scenario.  $PL_{0,dB}$ , the path loss value at the distance  $d_0 = 7$  cm, increase from 48.5 dB to 53 dB with the higher frequency band, which is because of the raising of conductivities of tissues, as implies in Fig. 3 (b). With the same reason, the path loss exponent,  $n$ , also increases from 4.54 to 6.24. The electromagnetic fields propagate through several different tissue layers, with different electrical properties, from the intra-heart to subcutaneous, which causes reflection and scattering at the interface of adjacent tissues. The standard derivation  $\sigma$  represents the concentration of the path loss values around its mean value. As listed in Table 1, the standard derivation  $\sigma$  of the fitted path loss models in WMTS band is larger than those of MICS and 868 MHz ISM bands, which indicate that the reflection and scattering are larger.

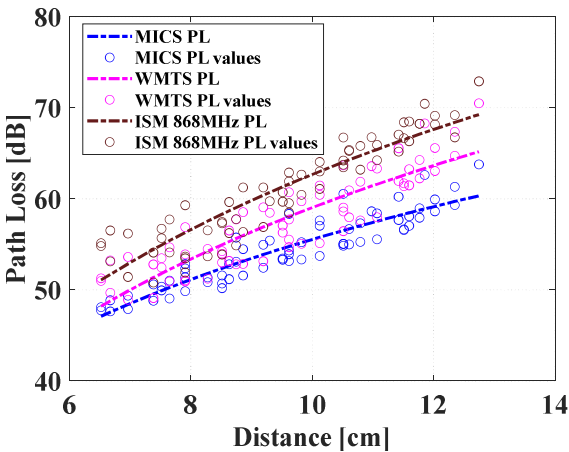


**Figure 5.** Intra-Cardiac to Subcutaneous path loss values and model at (a) MICS Band (402 – 405 MHz), (b) WMTS Band (608 – 614 MHz) and (c) 868 MHz ISM Band (867 – 869 MHz).

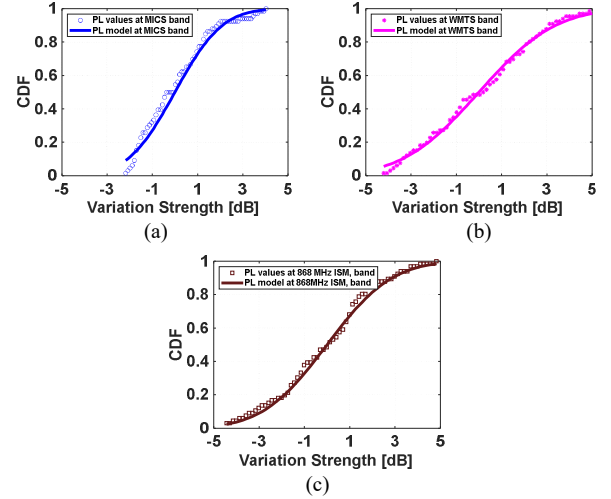


**Figure 6.** CDF of variation strength of Intra-Cardiac to Subcutaneous path loss model at (a) MICS Band (402-405 MHz), (b) WMTS Band (608-614 MHz) and (c) ISM Band (867-869 MHz).

**Table 1.** Summary of the parameters of the path loss models for intra-cardiac to subcutaneous

Parameter	MICS Band	WMTS Band	868 MHz ISM Band
$d$ [cm]	6 – 13	6 – 13	6 – 13
$f$ [MHz]	402 – 405	608 – 614	867 – 869
$PL_{0,dB}$	48.5	50	53
$d_0$ [cm]	7	7	7
$n$	4.54	5.83	6.24
$\mu$	0	0	0
$\sigma$	1.64	2.64	2.24

For intra-cardiac to off-body channel, the path loss values and fitted model are shown in Fig. 7 and Fig. 8, and the parameters are summarized in Table 2. The range of the distance from transmitting antenna to receiving antenna is approximate from 8 cm to 26 cm. The intra-cardiac to off-body channel can be divided into two paths: intra-cardiac to on-body and on-body to off-body. As shown in Fig. 7, when the distance is less than 16 cm, the variations of path loss values are large. And after 16 cm, the simulated path loss values approximately overlap with the fitted models, especially at WMTS and 868 MHz ISM bands. This is because that when the distance is larger than 16 cm, the reflection, scattering and diffraction, caused by the human body, becomes less and the path loss is dominated by the free space loss. Table 2 implies that the  $PL_{0,dB}$ , the path loss at the distance  $d_0 = 8$  cm, increases with the higher frequency band, which is because that when the distance is less, the loss caused by the human tissue dominates. The path loss exponent,  $n$ , is largest at WMTS band compared with that at MICS and 868MHz ISM bands and the path loss at WMTS band becomes larger than that at 868 MHz ISM band after 16 cm of the distance, which tells that to reduce the path loss from intra-cardiac to subcutaneous, the frequency level is not the only factor that should be considered.

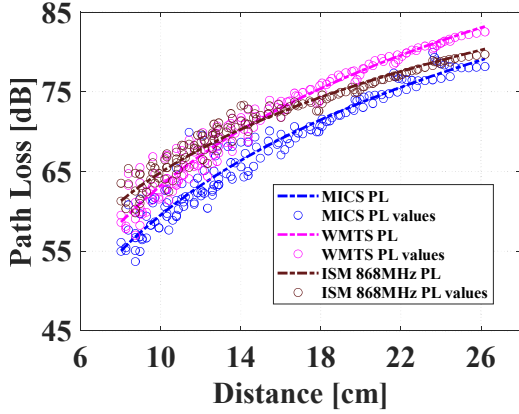


**Figure 7.** Intra-Cardiac to Off-Body path loss values and models at three sub-one GHz frequency bands.

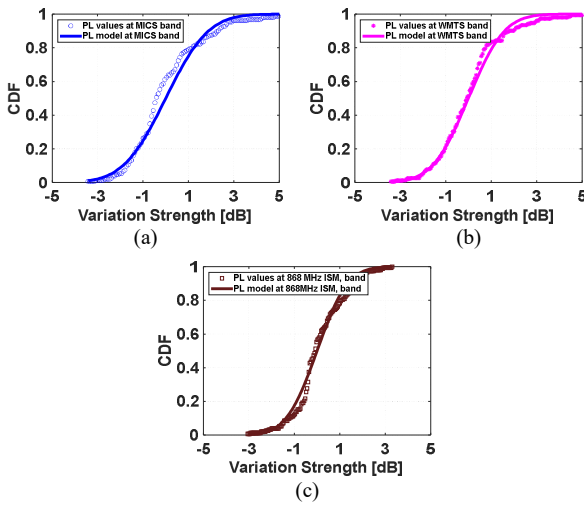


**Figure 8.** CDF of variation strength of Intra-Cardiac to Off-Body path loss modes at three sub-one GHz frequency bands.

**Table 2.** Summary of the parameters of the path loss models for intra-cardiac to off-body

Parameter	MICS Band	WMTS Band	868 MHz ISM Band
$d$ [cm]	8 – 26	8 – 26	8 – 26
$f$ [MHz]	402 – 405	608 – 614	867 – 869
$PL_{0,dB}$	55	58.6	61.3
$d_0$ [cm]	8	8	8
$n$	4.68	4.78	3.70
$\mu$	0	0	0
$\sigma$	1.48	1.25	1.06

## 4 Conclusions

This paper presents the numerically analyzed narrow band sub-GHz path loss models of intra-cardiac to subcutaneous and intra-cardiac to off-body for the leadless pacemaker applications. We observed that, for the intra-cardiac to subcutaneous channel, the loss, reflection and scattering caused by human body mainly influence the path loss models. The path loss increases with the raising of level of frequency band and the standard derivation of the fitted path loss model is largest at WMTS band. For the intra-

cardiac to off-body channel, not only the loss caused by the human tissue but also the diffraction and free space loss should be taken into consideration for the path loss models. These proposed models can facilitate the design and evaluation of the transceiver and receiver, synchronization schemes, etc.

## 5 Acknowledgements

This research is supported by "WiBEC" (Wireless In-Body Environment) project and "MEDICOS" (Smart Implants – Adaptive Communication and Biosignal Processing Systems) project

## 6 References

1. H. G. Mond, and Alessandro Proclemer. "The 11th world survey of cardiac pacing and implantable cardioverter-defibrillators: calendar year 2009—a World Society of Arrhythmia's project." *Pacing and clinical electrophysiology* 34, no. 8 (2011): 1013-1027.
2. A. Khaleghi, R. Chávez-Santiago, X. Liang, I. Balasingham, V. C. M. Leung, and T. A. Ramstad. "On ultra wideband channel modeling for in-body communications." In *IEEE 5th International Symposium on Wireless Pervasive Computing 2010*, pp. 140-145. IEEE, 2010.
3. M. Maldari, M. Albatat, J. Bergsland, Y. Haddab, C. Jabbour, and P. Desgreys. "Wide frequency characterization of Intra-Body Communication for Leadless Pacemakers." *IEEE Transactions on Biomedical Engineering* (2020).
4. P. Bose, A. Khaleghi, and I. Balasingham. "In-body and off-body channel modeling for future leadless cardiac pacemakers based on phantom and animal experiments." *IEEE Antennas and Wireless Propagation Letters* 17, no. 12 (2018): 2484-2488.
5. C. Gabriel, "Compilation of the dielectric properties of body tissues at RF and microwave frequencies," *Brooks Air Force*, N.AL/OE-TR-1996-0037, San Antonio, TX, 1996